



Analytical and Experimental Investigation of the Electrical-Thermal Behaviour of Electrical Contact Systems

Michael Blauth^{1,2,3}, Frank Berger² and Jian Song^{1*}

¹Ostwestfalen-Lippe University of Applied Science, Liebigstraße 87, 32657 Lemgo, Germany.

²Ilmenau University of Technology, Gustav-Kirchhoff-Straße 1, 98693 Ilmenau, Germany.

³Phoenix Contact GmbH & Co. KG, Flachsmarktstraße 8, 32825 Blomberg, Germany.

Authors' contributions

All authors read and approved the final manuscript.

Research Article

Received 25th June 2013

Accepted 7th August 2013

Published 1st October 2013

ABSTRACT

The current carrying capacity, which is determined by the electrical-thermal behaviour, is one of the main features of an electrical contact system.

The purpose of this study is to develop an analytical model which describes the electrical-thermal behaviour of electrical contact systems.

Established mechanical, electrical, thermal and contact physical relations are combined to design the analytical model. Differential equations with appropriate boundary conditions are used to solve the heating problem.

The various parts of an electrical connector represent separate subsystems. The geometry, the material properties and the heat transfer coefficients for the contact system, the terminal clamp and the wire have been taken into account. These different subsystems have been connected to obtain the overall temperature distribution.

In order to verify the analytical model, contact systems made of three copper alloys with different electrical and thermal properties are investigated experimentally at various current loads.

It was shown that the analytical model can predict the temperature rise for simple geometry well.

Using the analytical model several parameters can be easily changed. Moreover, the main influencing factors and their relationships can be identified directly on the equations. Therefore, the physical - mathematical point of view of an analytical calculation can help

*Corresponding author: E-mail: jian.song@hs-owl.de;

to understand the model structure of a contact system.

Keywords: *Analytical calculation; electrical contacts; contact physics; electric conductivity; heating; thermal behaviour.*

ABBREVIATIONS

Symbols		Indices	
A	Area	0,1,2	Variables
a	Radius of contact area	20	At reference-temperature (20 °C)
	Parameters	b	Bulk
b	Location constant	C	Constriction
d	Diameter	calc	Calculated
	Differential	char	Characteristic
E	Young's modulus	cnd	Conduction
F	Force	conv	Convection
g	Gravitational acceleration (9.81 m/s ²)	cp	Heat capacity
Gr	Grashof number	el	Electrical
H	Hardness	Elastic	
h	Height	env	Environment
I	Current	f	Fluid
l	Length	i	Insulation
k	Factor depending on the skin effect	in	In
L	Lorenz coefficient (2.4×10^{-8} V ² /K ²)	K	Contact Point
n	Number	kin	Kinematic
Nu	Nusselt number	m	Average
P	Power	max	Maximal
Pr	Prandtl number	meas	Measured
Q'	Heat flux	mech	Mechanical
r	Radius	out	Out
R	Resistance	P	Contact Pin
Ra	Rayleigh number	rad	Radiation
Rm	Tensile strength	S	Spring
Rp0,2	Yield strength	s	Surface
T	Absolute temperature	T	Terminal Clamp
t	Time	th	Thermal
	Thickness	U	Perimeter
U	Voltage	W	Wire
	Perimeter	x	Variable
w	Width		Distance
x	Distance		At infinity
α	Heat transfer coefficient		
	Temperature coefficient		
Δ	Difference		
ε	Emissivity		
θ	Super-temperature		
ϑ	Temperature		
λ	Conductivity		
v	Poisson's ratio		
	Viscosity		
ρ	Specific electrical resistivity		
σ	Stefan-Bolzmann constant (5.669×10^{-8} W/(m ² *K ⁴))		
	Standard deviation		

1. INTRODUCTION

Numerical simulations by means of the Finite Element Analysis (FEA) are widely used to carry out the analysis of the electrical-thermal behaviour of electrical contacts. This method is very common in industry because it considers several physical effects [1]. It leads to an accurate forecast of the performance, even for very complex systems with many parameters. Several numerical studies were carried out using the Finite Element Analysis to analyse the thermal behaviour of electrical connectors [2,3,4,5].

On the other hand, an analytical analysis can provide the relationship between the electrical-thermal behaviour of an electrical contact system and the influencing parameters in a way which clearly reveals the relevance of every parameter. This is an important basis for a rational optimization of contact systems.

Once the structure of the analytical model is set with general solutions, the parameters can be varied within a wide range.

This is not always possible in the case of a numerical calculation with the Finite Element Analysis because not all the background and boundary conditions are known and therefore the validity of the calculation is always limited to a certain range of parameters.

In order to calculate the electrical-thermal behaviour of a contact system, phenomena from different physical fields have to be considered. Detailed studies in the physical fields of mechanics, electrics, thermal and contact physics can be found in the literature for electrical contacts [6,7,8,9].

Rudimental calculations have been conducted to calculate the temperature rise of a contact system analytically. Holm [6] introduced an approach for calculating the temperature of a bus-bar contact. Brenner [10] used the approach which was described in Holm and extended the calculation by the insulation of the wire. The power dissipation of the constriction resistance and the bulk resistance of the contact system were taken into account, however only the temperature rise of the wire was given, without regarding the temperature profile at the contact system.

These approaches were modified and combined in [11]. A contact system was set in a model which included the relevant physical parameters and appropriate boundary conditions.

In this study the contact system and the boundary conditions are explained in detail. Additionally the super-temperature in the contact area is considered, the analytical model is verified by the measured and calculated constriction resistance and a parameter variation is conducted.

The temperature rise is calculated for steady-state conditions using direct current and it is assumed that the contact point is the heat spot.

2. ANALYTICAL APPROACH

The analytical approach to calculate the temperature is based on the first law of thermodynamics (conservation of energy). The balance equation considers the different modes of the heat transfer (conduction, convection and radiation).

Assuming a constant cross-section area for a volume element (see Appendix), the energy balance yields to an ordinary differential equation of the second order [12]:

$$\frac{\partial^2 \vartheta}{\partial x^2} - \frac{\alpha_{\text{conv_rad}} * U}{\lambda_{\text{th}} * A_x} * (\vartheta(x) - \vartheta_{\text{env_}\infty}) + \frac{k * I^2}{\lambda_{\text{el}} * \lambda_{\text{th}} * A_x^2} = 0 \quad (1)$$

where $\alpha_{\text{conv_rad}}$ is the heat transfer coefficient (film coefficient) for convection and radiation, U the perimeter of the volume element, $\vartheta(x)$ the temperature at a specific point x , λ_{th} the thermal conductivity, λ_{el} the electrical conductivity, $\vartheta_{\text{env_}\infty}$ the temperature of the fluid at infinity, A_x the cross-section area, k a factor depending on the skin effect which can be assumed as $k = 1$ because only direct current is regarded, and I the rated current.

The general solution of equation (1) describes the temperature distribution $\vartheta(x)$ along a volume element [12]:

$$\vartheta(x) = a_1 * e^{(\frac{x}{b})} + a_2 * e^{(-\frac{x}{b})} + \vartheta_{\text{env_}\infty} + \frac{I^2}{\alpha_{\text{conv_rad}} * U * \lambda_{\text{el}} * A_x} \quad (2)$$

where a_1 and a_2 are two parameters which have to be determined by appropriate boundary conditions.

For an exponential function (first two terms in equation (2)), the location constant b describes the distance x , where the temperature decreases to $1/e \approx 36.8\%$:

$$b = \sqrt{\frac{\lambda_{\text{th}} * A_x}{\alpha_{\text{conv_rad}} * U}} \quad (3)$$

The heat transfer coefficient for radiation and convection $\alpha_{\text{conv_rad}}$ is to be determined. The calculation will be carried out separately in section 3.3.

The sum of the two last terms in equation (2) describes the offset temperature $\vartheta_{b_}\infty$ of the volume element. This is the temperature of a sufficiently long volume element, if no axial heat flux occurs. It is independent of the location x .

If an axial heat flux $d\dot{Q}_{\text{cnd_in}}$ (e.g. power dissipation of the constriction resistance) is induced on one side of the volume element, the temperature decreases according to an exponential function with the increasing distance from the heat source [13].

The distribution of the temperature difference between the location x and the far end of the cable which can be defined as the super-temperature $\theta(x)$ is described by:

$$\theta(x) = \vartheta(x) - \vartheta_{b_}\infty = a_1 * e^{(\frac{x}{b})} + a_2 * e^{(-\frac{x}{b})} \quad (4)$$

2.1 Boundary Conditions

In order to calculate the temperature distribution along the volume element, equation (4) has to be solved by extracting the unknown parameters a_1 and a_2 . Therefore, two boundary conditions have to be defined.

Two boundary conditions of second order (Neumann's boundary conditions) [14] have been used.

The first boundary condition defines the induced heat flux by conduction $d\dot{Q}_{cnd_in}$ on one side of the volume element (Appendix). This heat flux can be caused by the dissipative power of the constriction resistance.

The second boundary condition defines the distance x from the heat source where the heat flux is decayed. In this study it is assumed that the heat flux is decayed at the distance of $x = 5*b$. The distance can also be increased, but the change in the result is negligible.

3. MODEL OF THE CONTACT SYSTEM

For calculating the temperature of the contact system, different parts of the connector have to be considered.

The electrical connector consists of an electrical contact (two springs and a contact pin) and two terminal clamps. A wire including the insulation is fixed at each side (Fig. 1).

At the end of the contact pin and at the tip of the springs measuring pins are designed to measure the voltage drop on the contact point respectively, this being constriction resistance.

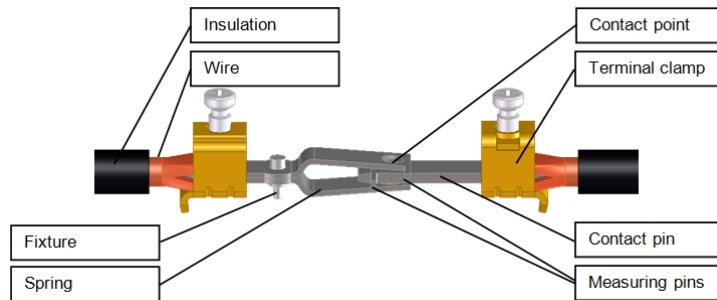


Fig. 1. Components of a connector

The springs, the contact pin, the terminal clamp and the wire have different materials, geometry and heat transfer coefficients. Hence, the location constant b must be calculated separately for every single component. In order to determine the temperature of the subsystems they have to be coupled by the heat flux \dot{Q}_x .

Fig. 2 shows the different subsystems. Each subsystem is represented by one volume element. The dissipative power at the constriction resistance induces the heat flux \dot{Q}_C into the contact pin. At the contact pin a specific temperature profile is built up which is defined by the location constant b_P . Due to heat conduction a heat flux \dot{Q}_{P_cnd} flows out of the contact pin into the terminal clamp and the heat flux \dot{Q}_{T_cnd} flows into the wire. Additionally, at every subsystem an individual heat flux ($\dot{Q}_{P_conv_rad}$, $\dot{Q}_{T_conv_rad}$, $\dot{Q}_{W_conv_rad}$) dissipates due to convection and radiation.

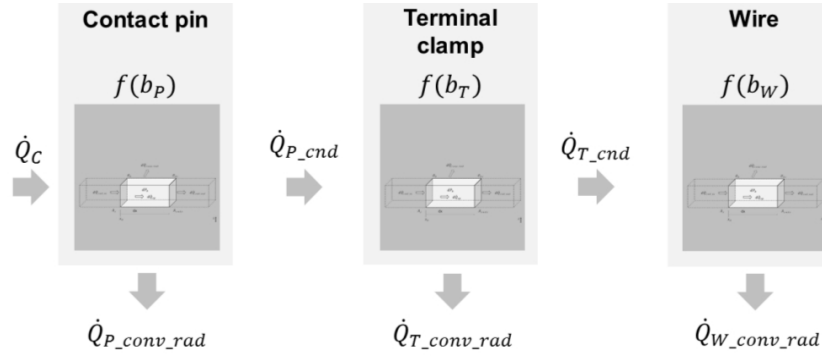


Fig. 2. Subsystems connected by the heat flux

According to Holm [6] superposition is valid to calculate the maximum temperature. Thus the separate temperature profiles of the different components are summed up.

Fig. 3 illustrates the schematic temperature profile and the separate temperatures for one side of the contact system (pin side). The temperature ϑ_C is the maximal temperature of the contact system in the contact interface. Technically it is not possible to measure this temperature at the contact system experimentally. $\vartheta_{P,\text{max}}$ is the maximal temperature on the surface of the contact pin in the vicinity of the contact area which can be measured.

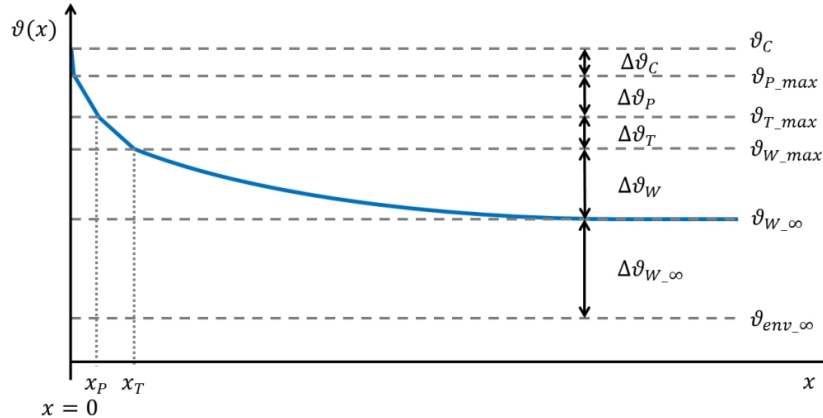


Fig. 3. Schematic temperature distribution in the electrical system for the pin side

$\Delta\vartheta_{W,\infty}$ is the temperature rise of the wire in infinity, $\vartheta_{W,\infty}$ the temperature of the wire in infinity, $\Delta\vartheta_W$ the change in temperature at the wire due to the axial heat flow, $\vartheta_{W,\text{max}}$ the maximal temperature of the wire at the interface to the terminal clamp at the point x_T , $\vartheta_{T,\text{max}}$ the maximal temperature of the terminal clamp at the interface to the contact pin at the point x_P , $\Delta\vartheta_T$ the change in temperature at the terminal clamp, $\Delta\vartheta_P$ the change in temperature at the contact pin, and $\Delta\vartheta_C$ the super-temperature in the contact area, according to Kohlrausch [18].

3.1 Temperature Rise of the Wire

As shown in equation (2) the offset temperature $\vartheta_{b-\infty}$ of the volume element can be calculated separately. In equation (2) the insulation is not considered. Therefore, the temperature of a wire with insulation is calculated separately. The temperature rise on the outer side of the insulation $\Delta\vartheta_{i-\infty}$ can be calculated as [14]:

$$\Delta\vartheta_{i-\infty} = R_w * I^2 * \frac{1}{a_{conv_rad_i} * A_i} \quad (5)$$

where R_w is the electrical resistance of the bulk material and A_i the heat emitting surface of the insulation.

The temperature rise at the internal side of the insulation is set as the temperature rise of the wire $\Delta\vartheta_{w-\infty}$:

$$\Delta\vartheta_{w-\infty} = \Delta\vartheta_{i-\infty} + R_w * I^2 * \left(\frac{\ln\left(\frac{r_i}{r_w}\right)}{\lambda_{th_i} * 2 * \pi * l_w} \right) \quad (6)$$

where r_i is the outer radius of the insulation, r_w the radius of the wire, λ_{th_i} the thermal conductivity of the insulation and l_w the length of the wire.

A linear relation can be assumed up to 100°C to calculate the temperature dependent electrical resistance for the bulk material [15]:

$$R(\vartheta) = R_{20} * (1 + \alpha_{th} * \Delta T) \quad (7)$$

where R_{20} is the electrical resistance at reference temperature (20 °C), α_{th} the temperature coefficient of resistance and ΔT the temperature rise of the bulk material.

3.2 Calculation of the Dissipative Power at the Constriction Resistance

In order to determine the temperature distribution in the contact pin the axial heat flux \dot{Q}_c , which is induced into the contact pin and the springs, has to be calculated. This axial heat flux is induced by the power loss of the constriction resistance between the contact spring and the contact pin.

The spring can be abstracted as a beam in bending with constant cross-section. In order to calculate the normal force F_K at the contact point, the geometric dimensions, material properties and the deflection of the spring x_{S1} have to be considered [16]:

$$F_K = \frac{E_S * w_S * h_S^3}{4 * l_S^3} * x_{S1} \quad (8)$$

where E_S is the Young's modulus of the spring, w_S the width of the spring and h_S the height of the spring. The mechanical length of the spring l_S is measured from the middle of the fixture point to the contact point (Fig. X2 in the Appendix).

The surface around the contact area of the contact system can be simplified as a contact of a sphere with the diameter d_K on a plane.

The radius of the contact area a_{el} can be calculated by the Hertz's contact theory [17]:

$$a_{el} = \sqrt[3]{\frac{3 * F_K * (1 - v^2) * d_K}{4 * E_S}} \quad (9)$$

where v is the Poisson's ratio and E_S the Young's modulus of the bulk material.

Some restrictions have to be made in order to be able to use equation (9). The contact point should only be elastically deformed and the roughness of the surface is neglected.

The current has to flow through the contact area at the contact point when passing from the contact pin to the contact spring. A constriction of the current lines occurs in the contact zone. For clean metal contacts the contact resistance for a semi-infinite solid can be described by the ellipsoid model of Holm [6].

The constriction resistance R_C for one contact point is calculated by:

$$R_C = \frac{\rho}{2 * a_{el}} \quad (10)$$

where ρ is the specific electrical resistivity of the base material.

The dissipative power of the constriction resistance R_C leads to the axial heat flux \dot{Q}_C .

Due to symmetry, the constriction resistance and the heat flux are the same for both springs and the contact pin.

The number of springs n_S influences the number of contact points. Hence, the number of springs must be considered for calculating the heat flux:

$$\dot{Q}_C = \frac{1}{2 * n_S} * R_C * I^2 \quad (11)$$

Fig. 4 shows the different analytical models and their parameters of influence.

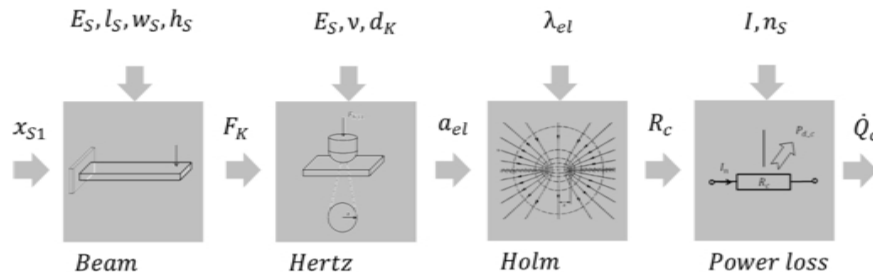


Fig. 4. Models for calculating the heat flux

The temperature in the contact interface ϑ_C is higher than the surface temperature of the bulk material (Fig. 3). The super-temperature $\Delta\vartheta_C$ is the deviation of the temperature in the contact interface ϑ_C from the bulk temperature ϑ_{P_max} . It can be calculated by the voltage-temperature relationship according to Kohlrausch [18]:

$$\Delta\vartheta_C = \frac{U_C^2}{8 * \rho * \lambda_{th}} = \frac{R_C^2 * I^2}{8 * \rho * \lambda_{th}} \quad (12)$$

U_C is the contact voltage due to the constriction resistance.

This equation is valid for monometallic electrical contacts and under the assumption that the heat within the contact area only dissipates by conduction.

The temperature decrease to that of the bulk over a distance of only several constriction diameters [8].

3.3 Calculation of the Heat Transfer Coefficients

The heat transfer rate $\dot{Q}_{\text{conv_rad}}$ is related to the temperature difference between the component ϑ_1 and the fluid $\vartheta_{\text{env_}\infty}$ and the surface area A_s . It is described by Newton's law of cooling [19]:

$$\dot{Q}_{\text{conv_rad}} = \alpha_{\text{conv_rad}} * A_s * (\vartheta_1 - \vartheta_{\text{env_}\infty}) \quad (13)$$

Convection and radiation are caused by different physical mechanisms. If they occur at the same surface they can be calculated separately and summed up [20].

So the total heat transfer coefficient $\alpha_{\text{conv_rad}}$ is the sum of the heat transfer coefficient for convection α_{conv} and the heat transfer coefficient for radiation α_{rad} :

$$\alpha_{\text{conv_rad}} = \alpha_{\text{conv}} + \alpha_{\text{rad}} \quad (14)$$

3.3.1 Convective heat transfer coefficient

Natural, or free, convection is observed as a result of motion of the fluid due to density changes arising from the heating process [19].

The convective heat transfer coefficient is not a physical material data [14]. It is also not always possible to obtain analytical solutions to convective problems [19]. For natural convection in particular, empirical relations are necessary to calculate the average convective heat transfer coefficient.

The convective heat transfer coefficient α_{conv} is calculated using the Nusselt number Nu , the characteristic length l_{char} and the thermal conductivity of the fluid $\lambda_{\text{th_f}}$ [20]:

$$\alpha_{\text{conv}} = \frac{\lambda_{\text{th_f}} * \text{Nu}}{l_{\text{char}}} \quad (15)$$

The Nusselt number depends on the geometry. Table 1 illustrates the equations employed to calculate the Nusselt number for a vertical plane and a vertical cylinder.

Thereby the validity of the equations is restricted to a specific range of the Rayleigh number under consideration.

Table 1. Nusselt number for free convection [14,20]

	Vertical plane	Vertical cylinder
Nusselt number	$Nu = \{0,825 + 0,387 * Ra * f_1(Pr)^{1/6}\}^2$ (16)	$Nu = \{0,752 + 0,387 * Ra * f_3(Pr)^{1/6}\}^2$ (17)
Influence of the Prandtl number	$f_1 * Pr = \left[1 + \left(\frac{0,492}{Pr}\right)^{9/16}\right]^{-16/9}$ (18)	$f_3 * Pr = \left[1 + \left(\frac{0,559}{Pr}\right)^{9/16}\right]^{-16/9}$ (19)
Characteristic length	$l_{char} = h$ (20)	$l_{char} = \frac{\pi}{2} * d$ (21)
Volume coefficient of expansion	$\beta = \frac{1}{T_{F_\infty}}$	(22)
Grashof number	$Gr = \frac{g * l_{char}^3 * \beta}{v_{kin}^2} * (\vartheta_1 - \vartheta_{F_\infty})$	(23)
Rayleigh number	$Ra = Gr * Pr$	(24)

*Restriction: $10^{-1} < Ra < 10^{12}$

**Restriction: $3,9 * 10^{-5} < Ra < 3,9 * 10^{12}$

where Pr is the Prandtl number, h the vertical length of the plane, d the cross-section diameter of the cylinder, T_{F_∞} the absolute temperature of the fluid in infinity, v_{kin} the kinematic viscosity of the fluid and g the gravitational acceleration.

The material properties for the fluid are temperature dependent (Table X1 in Appendix). They have to be used for the average temperature ϑ_m [20]:

$$\vartheta_m = \frac{1}{2} * (\vartheta_1 + \vartheta_{F_\infty}) \quad (25)$$

where ϑ_1 is the temperature of the object

3.3.2 Heat transfer coefficient for radiation

Thermal radiation is that electromagnetic radiation emitted by a body as a result of its temperature [19].

In order to calculate the heat flux, a small convex object enclosed by a very large concave surface is assumed. This corresponds to the test setup, since the tested components are enclosed by the test cabinet which is much larger than the size of the tested components [21]. Under these conditions the heat flux due to radiation can be calculated by [19]:

$$\dot{Q}_{rad} = A_s * \sigma * \epsilon_1 * (T_1^4 - T_2^4) \quad (26)$$

where σ is the Stefan-Bolzmann constant ($5,669 * 10^{-8}$ W/(m²*K⁴)), T_1 the temperature of the object, T_2 the temperature of the large concave surface and ϵ_1 the emissivity of the component.

In order to place the convection and radiation on a common basis (equation (13)) it is convenient to define a radiation heat transfer coefficient which is strongly temperature dependent [19]:

$$\alpha_{\text{rad}} = \sigma * \epsilon_1 * (T_1 + T_2) * (T_1^2 + T_2^2) \quad (27)$$

3.4 Energy Conservation at the Contact System

The offset temperature $\vartheta_{w,\infty}$ is only calculated for the wire. For the other components in the system the temperature distribution is calculated according to equation (4).

In the calculation different electrical conductivities for the contact pin and the contact spring are intended. Accordingly, different power losses are generated in the bulk materials. These losses are still not under consideration.

In order to improve the analytical model, conservation of energy is done separately at the contact pin and the terminal clamp.

The heat flux is generated by the constriction resistance, the bulk resistance of the contact pin and the spring and by the bulk resistance of the terminal clamps. The heat flux can dissipate by convection and radiation leaving the surface. In addition the heat flux $\dot{Q}_{T,\text{cnd}}$ dissipates by conduction into the wire (Fig. 2). So the accurate heat flux induced in the wire can be calculated separately.

If only axial heat flux from the constriction resistance is regarded, the heat flux into the wire becomes too low.

4. EXPERIMENTS

In order to verify the analytical calculations and to investigate the influence of the bulk material on the temperature rise of the contact system, contact systems with three different materials were investigated.

The different models were validated step by step. At first, the temperature of a quasi-infinite undisturbed wire without a contact system was investigated.

After calculating the temperature of the quasi-infinite wire, the temperature of a wire with a contact system was investigated. The same test setup was used.

The test setup is designed according to the DIN EN 60512-5-2 norm [21]. The temperature is measured by thermocouples of the type K. Only the stationary temperature is measured.

4.1 Test Wire

In the experiments a harmonised wire type H07V-K 35 mm² according to the DIN VDE 0281 norm [22] is used. The geometric data and the material properties are listed in Table X2 (Appendix)

The tests were conducted with direct current at three different current levels of 54 A, 98 A and 158 A.

The temperature T_w was measured at the bulk material in the inner side of the insulation and the temperature T_i was measured on the outer side of the insulation (Fig. 5).

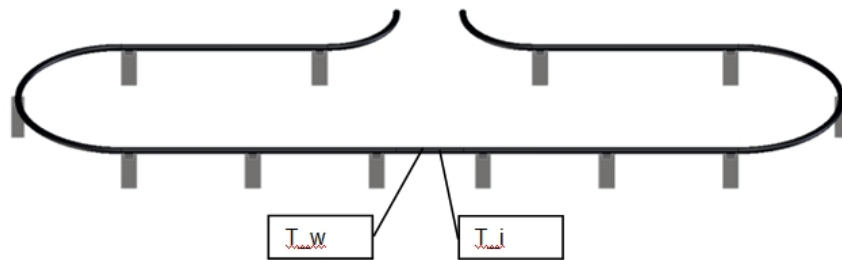


Fig. 5. Test setup for the wire

4.2 Test Connectors

Contact systems made of materials with three different electrical conductivities have been investigated. These contact systems have the same geometry and the same contact force. Only the electrical conductivity varies. The geometric properties are listed in Table X3 (Appendix).

The measured contact normal force for the spring is (10.5 ± 0.5) N, if the contact pin is inserted. Using the data from Table X3 and Table X4 (Appendix) the calculated contact normal force according to equation (8) is between 11.4 N and 11.8 N, depending on the Young's modulus. Thus the calculated values are somewhat higher than the measured ones because of the simplification of the mechanical model for the beam.

The electrical conductivity was measured at the components. Then the thermal conductivity was calculated according to the Wiedemann-Franz law [6]:

$$\frac{\lambda_{\text{th}}}{\lambda_{\text{el}}} = T * L \quad (28)$$

where L is the Lorenz coefficient $(2.4 \times 10^{-8} \text{ V}^2/\text{K}^2)$ and T is the absolute temperature.

Compared to other materials, pure copper and pure silver have the highest electrical conductivity of all metals at 20 °C (Ag: 62.9 MS/m, Cu: 60 MS/m [9]), respectively the highest thermal conductivity. Copper and copper alloys are commonly used as base materials for the current carrying parts in connectors [7]. The alloying elements strongly influence the electrical and mechanical properties of copper. Copper alloys have a higher mechanical strength than the pure copper, however the electrical conductivity of copper alloys is lower. A high alloyed copper may have an electrical conductivity which is comparable with iron or steel (Fe: 10 MS/m, CuSn6: 9 MS/m [9]).

In this study the copper alloys were selected because of their similar mechanical properties and different electrical and thermal properties. Their properties are listed in Table X4 (Appendix). These values were used for the calculation.

An oxidation film may form in the contact area which increases the contact resistance. The film resistance depends on the thickness and on the electrical conductivity of the film [9]. The film resistance may increase the power loss and therefore the temperature in the contact system. In order to minimize the influence of surface films, the contact systems are coated with a pure gold plating (0.75 ± 0.1) µm and a nickel under layer (2.25 ± 0.4) µm at the

contact area. Based on high corrosion resistance of gold, a metallic contact can be assumed and the whole contact area according to equation (9) can be regarded as the conducting contact area (a-spot) [6] without insulating impurities.

According to [9] the electrical resistance can be influenced by the coating. It depends on the relation between the coating thickness and the a-spot diameter. For the experiments the ratio between the layer thickness (2 µm) and the a-spot diameter (2 * 79 µm) is minimal (0.0125), thus the effect of the coating on the constriction resistance can be neglected.

The coefficient for emissivity depends on the state of the surface. For copper it can vary within a wide range (polished: $\epsilon = 0.03$; oxidized: $\epsilon = 0.76$ [20]). In order to have known and constant values for the calculation, the contact system and the terminal clamp are painted with black paint after assembling ($\epsilon = 0.92$).

Due to the relatively small temperature differences at the different components, the average heat transfer coefficient for the individual component is assumed for the calculation. The heat transfer due to convection and radiation is applied on all radial surfaces.

In Fig. X3 (Appendix) the calculated heat transfer coefficient for temperatures from 35°C to 100°C is depicted. The heat transfer coefficient for convection strongly depends on the geometry, the dimensions and the temperature. Within this temperature range the heat transfer coefficient for radiation is smaller than that for convection.

The wire is connected on the both sides of the contact pin and the contact spring (Fig. 2) in order to obtain the maximum contact area. Due to the large contact area and for simplification, the constriction resistance for the terminal clamp is neglected. For the calculation the assumed cross-section area for the terminal clamp is the average cross-section area of the contact pin, respectively the contact springs and the wire. The electrical and the thermal conductivities of the wire are almost constant for different types of wires. The material properties for a contact system may differ within a wide range. In the terminal clamp the properties of both components have to be considered. Therefore, the ratio of mixture for the two different materials is assumed to calculate the electrical and thermal conduction for the terminal clamp:

$$\lambda_T = \lambda_P * \frac{A_P}{A_P + A_W} + \lambda_W * \frac{A_W}{A_P + A_W} \quad (29)$$

where λ_T is the electrical / thermal conductivity of the terminal clamp, λ_P the electrical / thermal conductivity of the contact pin, λ_W the electrical / thermal conductivity of the wire, A_P the cross-section area of the contact pin and A_W the cross-section area of the wire.

The temperature close to the contact area is measured by thermocouple T_001 (Fig. 6). It is fixed as closely as possible to the contact area. At the wire the thermocouple T_045 to T_600 are fixed under the insulation to measure the bulk temperature. In order to determine the temperature distribution, the thermocouples are fixed at different distances to the contact point (45 mm, 100 mm, 200 mm, 300 mm, 400 mm and 600 mm).

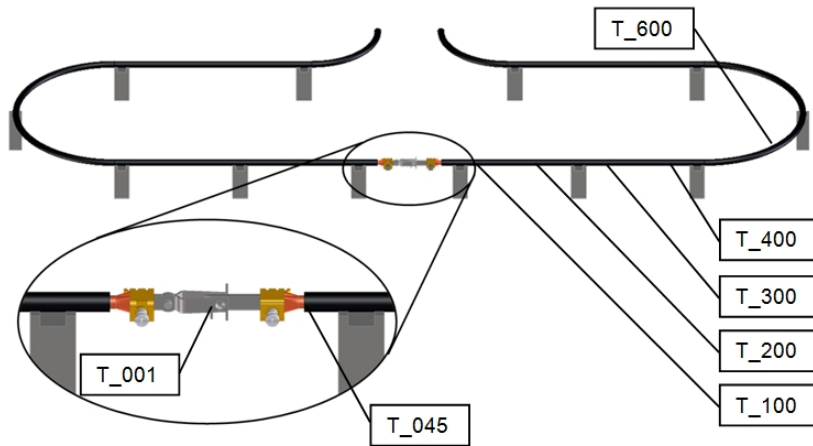


Fig. 6. Test setup for the connectors

5. RESULTS AND DISCUSSION

Fig. 7 shows the comparison of calculated and measured temperature rise depending on the rated current. The measured and calculated values both in the inner side of the insulation and in the outer side show a good correlation at different current levels. The difference is less than 1 K.

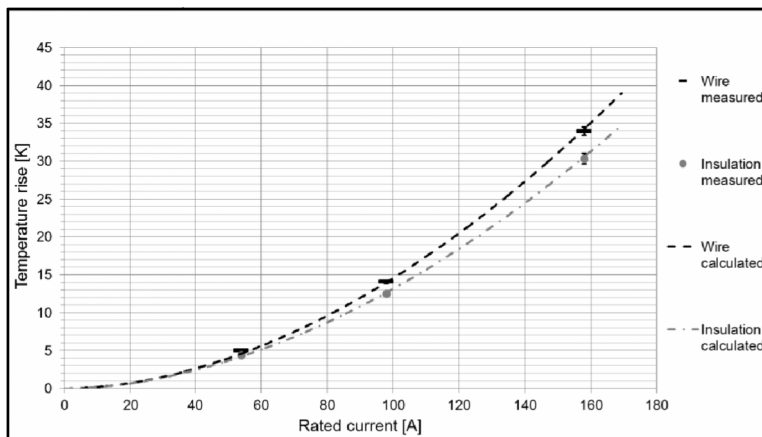


Fig. 7. Temperature rise of the wire
Wire: 35 mm^2 , $\vartheta_{\text{env}, \infty}: (26 \pm 1)^\circ\text{C}$, Range of the temperature rise: $\pm 1\sigma$ (Standard deviation)

The good correlation between the measured and calculated temperature can only be achieved if temperature dependent material values and heat transfer coefficients are used for the calculation. This means that an iterative calculation is necessary to obtain the temperature dependent values.

Fig. 8 shows the experimental results and the analytically calculated temperature distribution for the three different contact systems. For each test series five virgin contact systems were investigated.

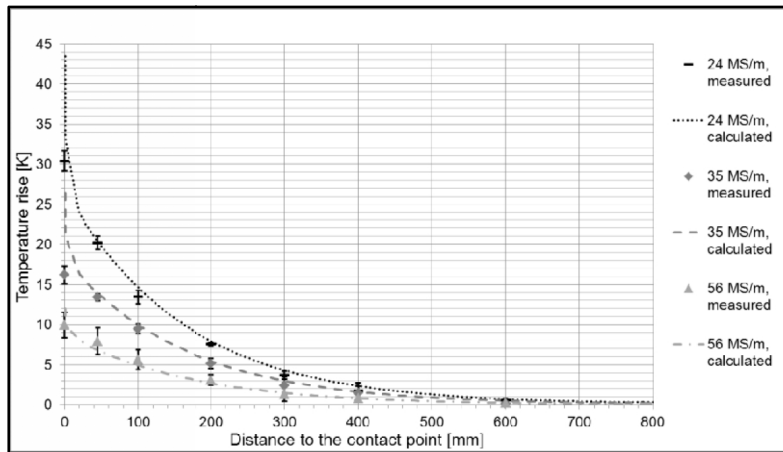


Fig. 8. Comparison of the calculated and measured values of the temperature rise

With calculated constriction resistance R_c_calc

Wire: 35 mm², Rated current: 158 A DC, $\vartheta_{env,\infty}$: (26 ± 1) °C,

Range of the temperature rise: ± 1σ (Standard deviation)

Qualitatively there is a good correlation between the calculated values with the measured ones. Along the wire (starting at a distance of 32 mm from the contact point) the exponential characteristic of the temperature distribution is visible.

At the contact pin a larger temperature gradient is calculated, which is similar to that for the wire. The reasons for this is the physically smaller cross-section area and the different electrical and thermal conductivities of the contact pins. The measured temperature gradient in the contact pin is slightly lower than the calculated temperature gradient. However, in the experiments the temperature is measured not directly in the contact point. The temperature there is of course somewhat lower than the temperature at the contact point.

The maximum temperature difference between measured and calculated values is 4 K for the temperature $\vartheta_{P,max}$ on the surface of the contact pin of the contact systems with electric conductivity of 24 MS/m, 5 K for the contact systems with electric conductivity of 35 MS/m and less than 1 K for the contact system with the electrical conductivity of 56 MS/m. The lower the electric conductivity of the contact systems the greater the inaccuracy of the calculated values. This also indicates that the difference between the measured and calculated values can be at least partly traced back to the distance between the measuring and contact point.

The calculated temperature values tend to be higher than the measured values. One reason for these discrepancies is a heat flux at the contact point which is assumed to be too high.

For calculating the heat flux, elastic deformation without plasticity was considered. So the calculated contact area is too small and the contact resistance too high. Additional roughness and softening in the contact area result in a real contact area that is higher than the calculated one, and thus a lower temperature occurs.

The calculation shows that the super-temperature ϑ_C in the contact area increases the maximum temperature at the contact system significant for highly stressed contact systems as those with 24 MS/m and 35 MS/m.

In order to verify the thermal model, the measured constriction resistance can be used instead of the calculated resistance.

The constriction resistance was measured at nominal current as near as possible to the contact area between the two measuring pins at the contact pin and the contact spring (Fig. 1).

Table 2 shows the comparison of the calculated and the measured constriction resistance.

Table 2. Constriction resistance

Electrical conductivity	λ_{el}	MS/m	24	35	56
Constriction resistance measured at 158 A	R_{c_meas}	mΩ	0,235	0,159	0,126
Standard deviation	$1 * \sigma$	mΩ	0,020	0,010	0,008
Constriction resistance calculated (Hertz / Holm) for 158 A	R_{c_calc}	mΩ	0,295	0,214	0,131

R_{c_meas} and R_{c_calc} are the constriction resistance for one contact point. The temperature of the constriction resistance is considered in the calculation.

There is a good correlation between the measured and calculated constriction resistance for the contact system with an electrical conductivity of 56 MS/m.

For the other two contact systems there is a discrepancy of between 26 % and 35 % in the contact resistance. This causes the difference in the calculated temperature.

The calculation of the temperature rise with the measured constriction resistance is shown in Fig. 9. There is a good correlation between the measured and calculated values.

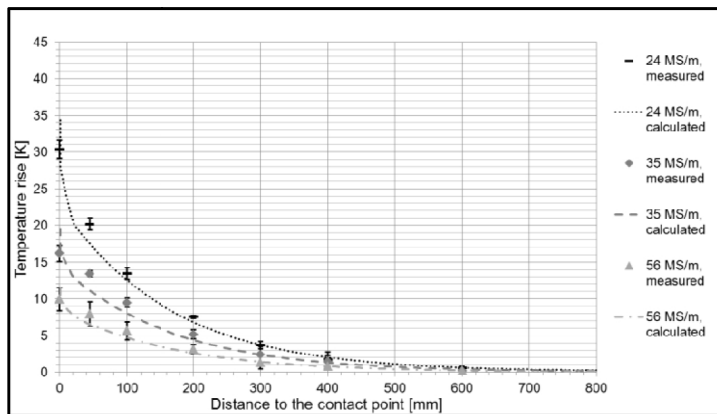


Fig. 9. Comparison of the calculated and measured values of the temperature rise

With measured constriction resistance R_{c_meas}

*Wire: 35 mm², Rated current: 158 A DC, $\vartheta_{env\infty}$: (26 ± 1) °C,
Range of the temperature rise: ± 1σ (Standard deviation)*

The calculated super-temperature ϑ_C is smaller because the assumed contact resistance has decreased.

The energy conservation at the contact system in section 3.4 presents the possibility to display the main causes of electrical power generation (Joule's heating) and heat dissipation (Emission due to convection, radiation and conduction).

For the contact system with an electrical conductivity of 56 MS/m approximately half of the power loss is created by the constriction resistance. The other half is generated by the bulk resistance of the contact system and the terminal clamp as shown in Fig. 10. One third of the generated power is induced into the wire.

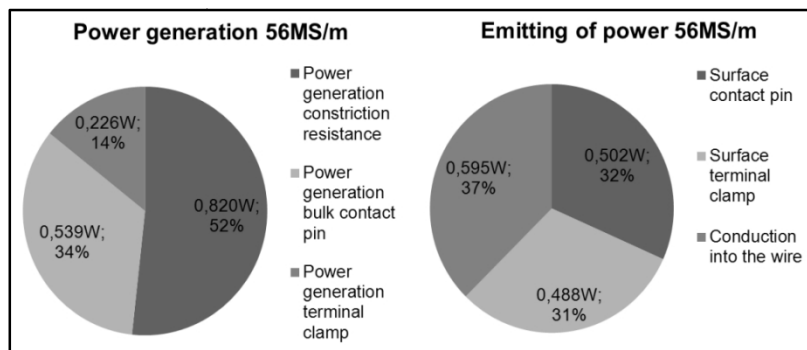


Fig. 10. Percentage of power loss
Contact system with 56 MS/m for rating current 158 A

The model used for the calculation can also be used to carry out the relevance ranking of the parameters for electrical-thermal behaviour of a contact system (Fig. 11).

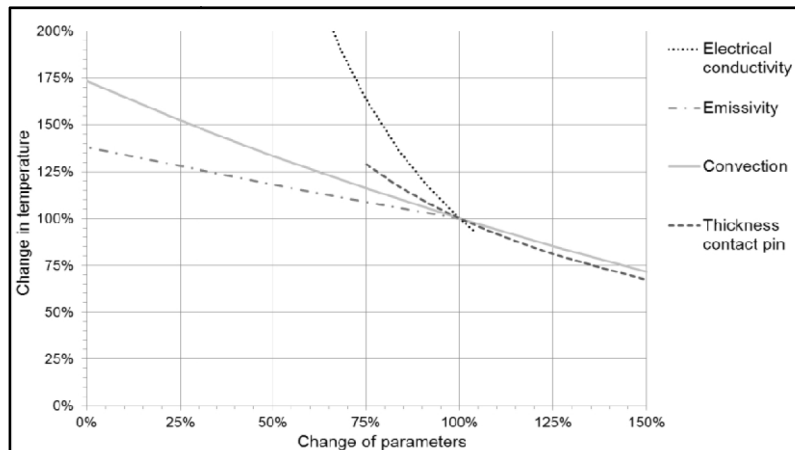


Fig. 11. Variation of several parameters
Reference (100 %): temperature: ($\vartheta_{P_max} - \vartheta_{W_\infty}$), wire: 35 mm², rated current: 158 A DC, electrical conductivity: 56 MS/m, ϑ_{env_∞} : (26 ± 1) °C

For the relevance ranking the temperature rise of the contact pin is considered (ϑ_{P_max} - $\vartheta_{W_∞}$ in Fig. 3). A constant current levels of 158 A is assumed, thus the temperature rise of the wire $\vartheta_{W_∞}$ is always the same.

The heat transfer coefficient of radiation and convection for the contact pin and the terminal clamp are varied. The thickness of the contact pin is varied while the contact force is held constant.

The electrical conductivity and the thickness of the electric contact influence the temperature rise and therefore the current carrying capability markedly, while the emission coefficient shows a minor influence on the electrical-thermal behaviour. Convection has a greater influence on the contact system than radiation because the absolute amount of heat transfer for convection is greater than that for radiation. If convection and radiation tend to zero, an adiabatic calculation is defined. Thus an adiabatic calculation has a significant influence on the accuracy for the temperature. This is not advisable because in that case all the generated power would be induced into the wire, which increases the absolute temperature.

4. CONCLUSION

An analytical model is introduced for the calculation of the electrical-thermal behaviour of electrical contact systems in which all components of a connector were considered. The challenge is to detail the analytical model enough to obtain accurate results. Modelling the contact point has a large impact.

For the investigated contact systems a good correlation between the measured and calculated temperatures was demonstrated by varying the current values and the electrical conductivities of the bulk material. The experiments confirmed the model.

One of the benefits of the model is that it clearly displays the relationship between the electrical-thermal behaviour and the parameters in the contact system. It aids the overall understanding of the contact system. A relevance ranking of parameters can be easily conducted to identify the importance of the parameters for the contact system. Only basic equations are used in the model for calculation of the contact area and the contact resistance. In order to achieve an exact result in every case, these sub-models must be improved. More accurate and complex models in combination with FEA and thermal networks which describe more details of a contact system will be developed during further studies.

COMPETING INTERESTS

Authors have declared that no competing interests exist.

REFERENCES

1. Gebhardt C. Praxisbuch FEM mit ANSYS Workbench. 1st ed. München: Hanser; 2011;84. German
2. Do TK, Cohen T. Coupled Thermal Electrical Finite Element Analysis of Power Contacts Used in High Speed Differential Connectors. 55th IEEE Holm Conference. September 14-16, 2009.

3. Angadi SV, Jackson RL, Choe S, Flowers GT, Lee BY, Zhong L. A Multi-physics Finite Element Model of a 35A Automotive Connector including Multiscale Rough Surface Contact. 56th IEEE Holm Conference. October 4-7, 2010.
4. Carvou E, El Abdi R, Razafiarivelo J, Benjema N, Zindine EM. Thermo-mechanical study of a power connector. In: Measurement. 2012;45:889–896.
5. Hauswald T. FEM Analysis Concept for Contact Systems. 4.th Symposium Connectors. March 6-7, 2013.
6. Holm R. Electric contacts. Theory and applications. 4th ed. Berlin: Springer; 2000:6,15,63,109,176.
7. Vinaricky E. Elektrische Kontakte, Werkstoffe und Anwendungen. 2nd ed. Berlin: Springer; 2002:297,407. German
8. Slade P. Electrical contacts. Principles and applications. New York: Dekker. 1999:47,52.
9. Braunovic M, Konchits VV, Myshkin NK. Electrical contacts. Boca Raton: CRC Press; 2007:160,211,588.
10. Brenner A. Anforderungen an Leistungssteckverbinder und Steckverbinder in der Informationselektronik. 15th Albert-Keil-Kontaktseminar "Kontaktverhalten und Schalten". September 22-24. 1999. German
11. Blauth M, Berger F, Song J. Berechnung der Stromtragfähigkeit von Kontakt-systemen. 4th Symposium Connectors. March 6-7. 2013. German
12. Philippow E. Taschenbuch Elektrotechnik Band 5. 1st ed. München: Hanser; 1981:777. German
13. Böhme H. Mittelspannungstechnik. 2th ed. Berlin: Huss-Medien; 2005:79. German
14. Marek R, Nitsche K. Praxis der Wärmeübertragung. 3th ed. München: Hanser; 2012:21,24,75,192. German
15. Lipsmeier A. Friedrich Tabellenbuch Elektrotechnik und Elektronik. 583th ed. Troisdorf: EINS; 2009. German
16. Meissner M, Wanke K. Handbuch Federn. 2nd ed. München: Verlag Technik, 1993:119. German
17. Johnson KL. Contact mechanics. 9th ed. Cambridge: Cambridge University Press; 2003:84.
18. Kohlrausch F. Über den stationären Temperaturzustand eines elektrisch geheizten Leiters. Annalen der Physik. 1900:132-158.
19. Holman JP. Heat transfer. 10th ed. Boston, Mass: McGraw-Hill Higher Education. 2010:10,277,327,379,412,460.
20. Verein Deutscher Ingenieure VDI-Gesellschaft Verfahrenstechnik und Chemieingenieurwesen. VDI-Wärmeatlas. 10th ed. Berlin: Springer; 2006. German
21. DIN EN 60512-5-2. Steckverbinder für elektronische Einrichtungen - Mess- und Prüfverfahren; 2003. German
22. DIN VDE 0281-3: Polyvinylchlorid-isolierte Leitungen mit Nennspannungen bis 450/750 V. 2001. German
23. Datasheet for Wieland-M10, Wieland-K65® and Wieland-K14® available at <http://www.wieland.de>

APPENDIX

Volume Element

A differential volume element with the length dx is depicted in Fig. X1. The balance equation considers the different modes of heat transfer (conduction, convection and radiation). These modes are described in [12].

In the bulk material with the length dx and the cross-section area A_x the dissipative power dP_b is generated internally by the Joule's heating because of the electrical current and the bulk resistance. On the surface A_x the axial conduction heat flux $d\dot{Q}_{cnd_in}$ flows into the volume element, and on the surface A_{x+dx} the heat flux $d\dot{Q}_{cnd_out}$ comes out of the volume element.

The surface of the volume element, respectively the perimeter U times the length dx , can emit the heat flux $d\dot{Q}_{conv_rad}$ through convection and radiation to the environment.

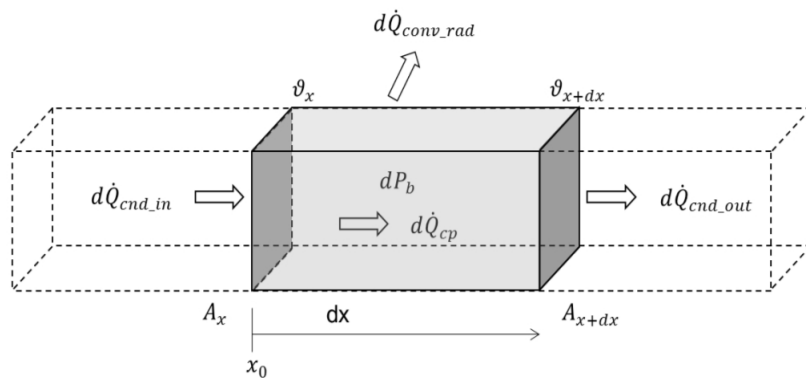


Fig. X1. Volume element for energy balance

θ_x in Fig. X1 is the temperature at the point $x=x_0$ and θ_{x+dx} the temperature at the point $x=x_0+dx$.

The heat capacity of the volume element is neglected because only the steady-state temperature is taken into consideration.

Table X1. Properties for air at pressure $p = 1$ bar [20]

Average temperature	θ_m	°C	30	40	50	60
Thermal conductivity	$\lambda_{th,f}$	mW/(m*K)	26.618	27.354	28.082	28.804
Kinematic viscosity	v_{kin}	10^{-7} m ² /s	162.6	172.3	182.2	192.2
Prandtl number	Pr	-	0.7068	0.7056	0.7045	0.7035

Table X2. Properties of the wire

Bulk radius wire	r_W_b	3.3	mm
Radius insulation	r_W_i	5	mm
Thickness insulation	t_W_i	1.2	mm
Length wire	l_W	1400	mm
Electrical conductivity wire	λ_{el_W}	58	$\text{m}/(\Omega^*\text{mm}^2)$
Thermal conductivity wire (at 20 °C)	λ_{th_W}	395	$\text{W}/(\text{m}^*\text{K})$
Temperature coefficient	α_{th_W}	4.3	$10^{-3}/\text{K}$
Thermal conductivity insulation	$\lambda_{th_W_i}$	0.17	$\text{W}/(\text{m}^*\text{K})$
Emission coefficient insulation	$\epsilon_{th_W_i}$	0.92	-

Table X3. Geometric properties for the contact system

Height contact pin	h_P	2.4	mm
Width contact pin	w_P	8.0	mm
Height spring	h_S	1.2	mm
Width spring	w_S	8.0	mm
Mechanical length spring	l_S_mech	26.0	mm
Radius contact point	r_K	4.0	mm
Spring deflection	x_S1	0.475	mm

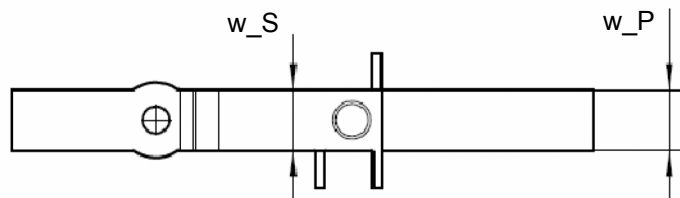
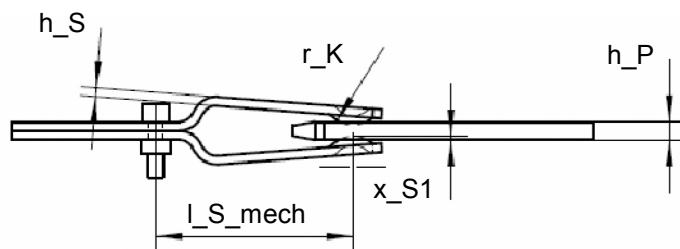


Fig. X2. Geometric size for the contact system

Table X4. Properties of materials for the contact system

Number	Material	Electrical ¹ conductivity		Thermal conductivity ²		Young's modulus ³	Yield strength ³	Tensile strength ³	Hardness ³	Coefficient of electrical resistance ³
		EN	λ_{el} MS/m	λ_{th} W/(m*K)	E GPa					
1	Cu-PHC	56	400	127	320	360	110	3.7		
2	CuFe2P	35	250	123	240	340	110	3.3		
3	CuZn10	24	172	124	290	350	110	1.8		

¹Measured with a Fischer SIGMASCOPE® SMP10

²Calculated according to equation (28) for $\vartheta_{env,\infty} = 25^\circ C$

³From the Datasheet [23]

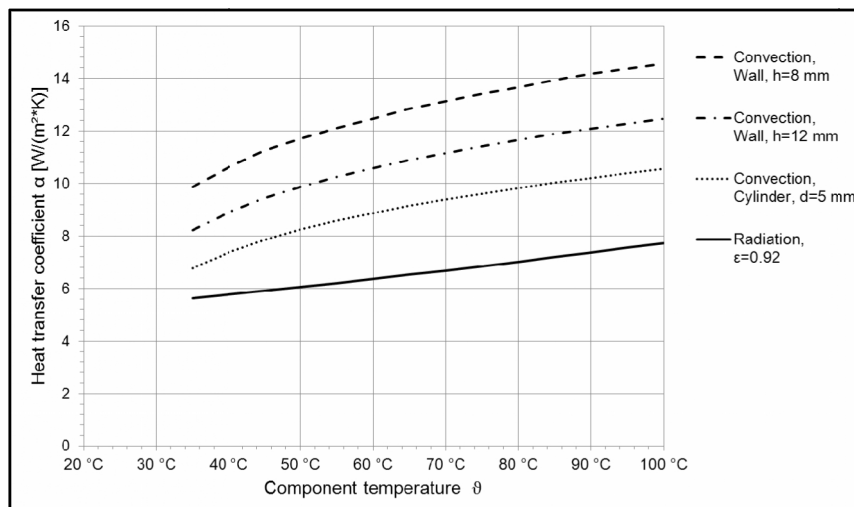


Fig. X3. Heat transfer coefficient for convection and radiation
 $\vartheta_{env,\infty}: 25^\circ C$

© 2014 Jian Song et al.; This is an Open Access article distributed under the terms of the Creative Commons Attribution License (<http://creativecommons.org/licenses/by/3.0>), which permits unrestricted use, distribution, and reproduction in any medium, provided the original work is properly cited.

Peer-review history:

The peer review history for this paper can be accessed here:
<http://www.sciedomain.org/review-history.php?iid=268&id=5&aid=2094>